Molecular Sensing Using Monolayer Floating Gate, Fully Depleted SOI MOSFET Acting as an Exponential Transducer

Bharath R. Takulapalli[†,*]

Center for Solid State Electronics Research, Science and Engineering of Materials, Arizona State University, Tempe, Arizona 85287. [†]Current address: Biodesign Institute, Arizona State University, Tempe, AZ 85287

ABSTRACT Field-effect transistor-based chemical sensors fall into two broad categories based on the principle of signal transduction—chemiresistor or Schottky-type devices and MOSFET or inversion-type devices. In this paper, we report a new inversion-type device concept—fully depleted exponentially coupled (FDEC) sensor, using molecular monolayer floating gate fully depleted silicon on insulator (SOI) MOSFET. Molecular binding at the chemical-sensitive surface lowers the threshold voltage of the device inversion channel due to a unique capacitive charge-coupling mechanism involving interface defect states, causing an exponential increase in the inversion channel current. This response of the device is in opposite direction when compared to typical MOSFET-type sensors, wherein inversion current decreases in a conventional n-channel sensor device upon addition of negative charge to the chemical-sensitive device surface. The new sensor architecture enables ultrahigh sensitivity along with extraordinary selectivity. We propose the new sensor concept with the aid of analytical equations and present results from our experiments in liquid phase and gas phase to demonstrate the new principle of signal transduction. We present data from numerical simulations to further support our theory.

KEYWORDS: field effect · sensors · pH sensing · exponential transduction · sensitivity · selectivity · FDEC

Current day science and technology has far surpassed human sensory capabilities of sight, sound, and touch, while electronic technologies that mimic sense of smell and taste have largely remained a challenge. The urgency for ultrahigh sensitive sensor devices for chemical, biological, radiological, nuclear, and explosive (CBRNE) detection in homeland security and military applications, and the paradigm of point-of-care diagnostics in future healthcare are two major drivers for advance research in chemical and biological sensors. Consequently, an increased number of new material technologies that are capable of label-free single molecule level sensing are reported.[1−3] However, none of the technologies available today satisfies all of the requirements for a robust sensing platform, *viz.* high sensitivity, high selectivity, reusability, inexpensive manufacturing, miniaturization, systems-on-chip integration capability, and so on. In this paper, we present a new field-effect device concept as a possible solution to some of these challenges in the field of chemical and biological sensing.

Field-effect sensors work on the general principle of detecting shifts in localized electric potential due to chemical interactions at the device surface. A chemical-sensitive thin film deposited on the device surface undergoes a specific chemical interaction with the target species, causing a change in the charge polarization inside the thin film and a corresponding shift in electrochemical potential at the device surface−thin film interface. The resultant change in electric field at the device surface modulates the density of charge carriers in the semiconductor conduction channel beneath it. In the case of chemiresistor or Schottky-type field-effect sensors,[4−8] the detection of target species is due to the field-effect modulation of channel *majority charge carrier density*, that is, chemical binding events at the device surface leading to accumulation and depletion of majority charge carriers in the semiconductor conduction channel. MOSFET-type sensors on the other hand are operated with the semiconductor channel biased in inversion.[9−11] In this type of device, target molecule binding at the chemical-sensitive device surface modulates the *minority charge carrier density* in the inversion channel. In either case, this Coulombic field-effect modulation of charge carriers in the conduction channel, characterized by the carrier Debye length, produces a corresponding change in conduction current measured across the

*Address correspondence to bharath.takulapalli@asu.edu.

Received for review July 31, 2009 and accepted January 5, 2010.

Published online January 19, 2010. 10.1021/nn900901f

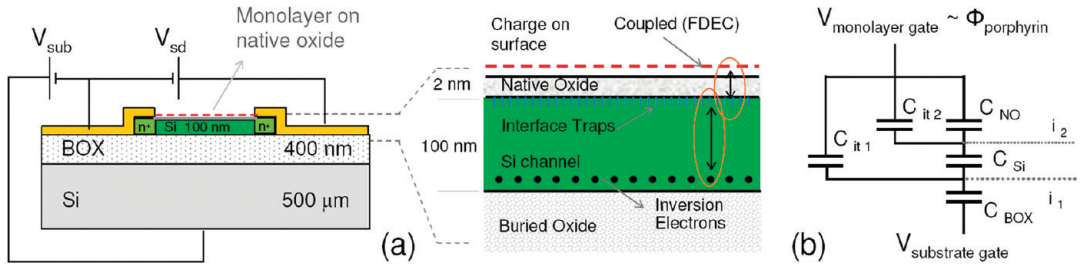

Figure 1. (a) Schematic of substrate gate SOI MOSFET with molecular monolayer deposited on native oxide (NO). Expanded view of the silicon channel depicts FDEC charge coupling of surface charge with inversion electrons at the bottom Si−BOX interface, indirectly *via* interface states at NO−Si interface. (b) Equivalent capacitance circuit of SOI MOSFET schematic.

channel source−drain regions, enabling the detection of target species.

When using SOI thin film field-effect devices in sensing applications, the top thin film silicon can be operated in four different regimes of interest: (1) in accumulation, (2) inversion with partial depletion of Si film, (3) inversion with full depletion of the Si film, and (4) in volume inversion mode where the whole of Si film is inverted. Our work discusses the device response in the case *of inversion with full depletion* of the Si thin film. We present here a new class of field-effect devices for chemical sensing applications, termed fully depleted exponentially coupled (FDEC) sensors using porphyrin monolayer floating gate fully depleted SOI MOSFET. In these novel MOSFET-based sensor devices, ligand binding at the device surface modulates the inversion threshold voltage of the device *via* a second-order capacitive charge-coupling mechanism involving interface defect states, resulting in an exponential increase in the device response. This response of the device is in opposite direction when compared to typical MOSFET-type sensors, wherein inversion current decreases in a conventional n-channel device upon addition of negative charge to the chemical-sensitive device surface.

A conventional thin film SOI MOSFET is a bi-gate structure with the silicon thin film sandwiched between top gate insulator and the buried oxide (BOX).[12,13] The substrate silicon contact acts as an additional gate with buried oxide (BOX) as its gate oxide. Unlike a regular MOS transistor, the thin film SOI transistor is a two interface problem, *viz.* top gate oxide−silicon channel interface and BOX−silicon thin film interface. When the silicon thin film is fully depleted, the two interfaces are strongly coupled, enabling control of either interface with its corresponding secondary gate. In our work, the SOI thin film is boron-doped (p-type 10^{15} cm^{-3}) 100 nm in thickness, and the top gate of the regular SOI MOSFET is replaced with zinc(II) 5,10,15,20-tetra(3-carboxylphenyl)porphyrin (ZnTCPP) molecular monolayer that now acts as a floating gate; details reported elsewhere.[14] Native oxide (NO) layer that is grown over the active silicon surface, underneath the molecular monolayer, acts as the corresponding monolayer gate oxide (Figure 1a). Electron inversion channel is established at the bottom silicon thin film−BOX interface by applying positive bias to the substrate silicon contact.

Analytical Model. Threshold voltage (V_t) of a conventional MOS transistor varies directly with the cumulative charge in the depletion region and at its boundaries, specifically charge at the Si channel−gate oxide interface. Variation of threshold voltage with charging and discharging of donor and acceptor-like interface trap states located at the gate oxide−silicon interface is well understood.[15] In our case of substrate-gate-biased fully depleted SOI FET, even charge at the native oxide (NO)−silicon interface, particularly due to interface states, needs to be considered in evaluating the threshold voltage of inversion channel formed at the bottom Si−BOX interface. When a net amount of charge is added to the molecular monolayer or to the surface of the native oxide, it causes charging and discharging of interface states at the NO−silicon film interface due to the high capacitance of the very thin native oxide layer,[15,16] *ca.* 2 nm. Addition of negative charge to the molecular monolayer causes charging of donor-like interface trap states (neutral when filled, below E_F) and discharging of acceptor-like interface charge states (neutral when empty, above E_F) in p-silicon, that is, a net increase of positive charge at the NO−Si interface. This in turn causes a decrease in threshold voltage of inversion channel formed at the Si−BOX interface according to $\Delta V_t \sim -\Delta Q/C_{eff}$, where ΔQ is the net charge added at the NO−Si interface and C_{eff} is the effective capacitance.

To get further qualitative understanding of the proposed coupling mechanism (Figure 2), let us approximate that the native oxide behaves as a thermal oxide with 2 nm thickness and dielectric constant $k_{ox} = 3.9$. Chemical binding of target molecule (amine) at the chemical-sensitive molecular monolayer (ZnTCPP) deposited on the native oxide causes reconfiguration of charges or shifts in the electrical dipole moments of the molecules in the monolayer. Any excess charge on the monolayer due to this is expected to be essentially immobile, acts as static charge, and is in equilibrium with molecular dipoles in the monolayer phase. When a negative charge (immobile) is added at the surface of the native oxide (or to the molecular monolayer), due

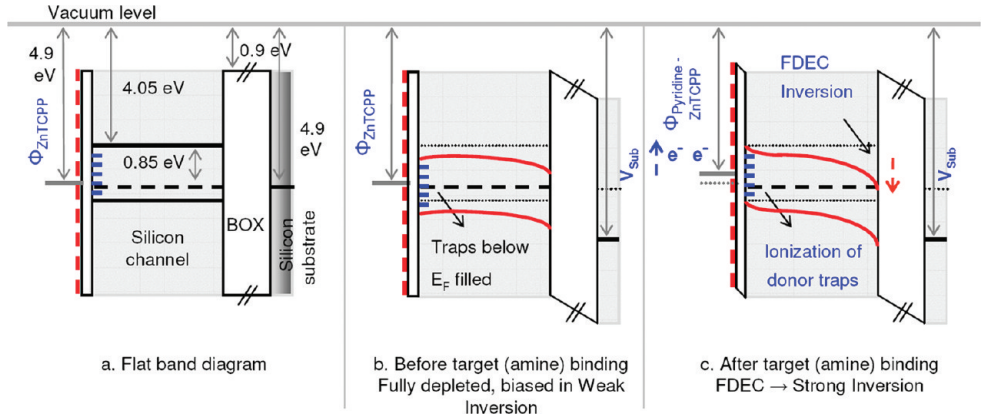

Figure 2. Schematic of energy band diagrams in the FDEC SOI MOSFET sensor device. (a) Flat band diagram with ZnTCPP monolayer and NO−Si channel shown to the left and Si−BOX interface to the right. (b) Device biased in weak inversion by applying positive substrate bias. The bands at the Si−BOX interface are pulled down past the intrinsic level, while bands in the fully depleted silicon channel and at the NO−Si interface follow. (c) Charge due to target molecule binding at the device surface tends to bend the bands upward at the NO−Si interface, causing discharge of electrons from donor traps or net increase in positive charge at the NO−Si interface. This excess interface positive charge drives the Si−BOX interface into inversion. In the schematic, band bending at the NO−Si interface is exaggerated for visual aid. In reality, Fermi level pinning tends to limit any band bending at the NO−Si interface.

to the high capacitance ($\sim 17.2 \times 10^{-7}$ F cm^{-2}) of the thin oxide, the silicon Fermi level "tends" to bend upward at the NO−Si interface (Figure 2c). In a p-type substrate (our device), this causes charging of donor interface states; that is, neutral traps lose electrons to gain positive charge (whereby pinning the Fermi level). If we approximate an interface trap state density of 5×10^{12} cm^{-2} eV^{-1} at the NO−Si interface, uniformly dispersed with respect to energy, a change in Si surface potential by 0.2 eV (band bending caused upon saturation of native oxide surface with electron charge from ligand binding) will result in 1×10^{12} cm^{-2} of extra positive charge at the NO−Si interface, which in turn results in a decrease in the inversion channel threshold voltage at the bottom Si−BOX interface. When biased in weak inversion, this threshold voltage decrease causes an exponential increase in device drain current. Due to the high density of interface charge at the NO−Si interface, Fermi level pinning occurs and band bending in silicon is expected to be localized to only a few nanometers (to the extent of the depth of the dangling bonds and other such defects at the NO−Si interface). Hence, we expect this unique charge coupling to occur only when the silicon film is fully depleted, while it behaves as a regular MOSFET-type sensor with standard Coulombic response (sensor current response in opposite direction) when partially depleted.

High densities of interface trap states exist at the NO−Si thin film interface. P_b densities of up to 2×10^{13} have been reported at the Si[111]−native oxide interface,[17,18] while the Si[100]−oxide interface is expected to have approximately a third of that.[19] A detailed study on interface charge generation−recombination at ultrathin thermally grown silicon dioxide−silicon interface as a function of oxide field strength and surface potential has been reported by Ogawa *et al.*[16] Effect of back gate interface trap density and back gate fixed charge density on front gate threshold voltage has been analyzed by Balestra *et al.* for the case of p-channel MOSFET.[20] Hovel has discussed in detail the variation with time of the inversion threshold voltage for *in situ* native oxide growth over the top silicon surface of the Hg-FET pseudo-MOSFET.[21] For a more rigorous analysis of the proposed capacitive coupling between the charge on the surface of native oxide and the surface potential at the Si−BOX interface, where the inversion channel is established, let us consider the equivalent capacitance circuit in Figure 1b. The BOX−silicon thin film interface is denoted as interface one (i_1) and the NO−Si interface as interface two (i_2). Threshold voltage of electron inversion channel at the Si−BOX interface ($V_{t\text{-}sub}$) can be written in terms of the individual element capacitances using the linearly varying potential (LVP) model as[22]

$$V_{t\text{-}sub} = V_{FB\text{-}G1} + \frac{2\Phi_F}{C_{Si} + C_{NO} + C_{it2}}\left[C_{Si} + C_{NO} + \frac{C_{NO}}{C_{BOX}}(C_{Si} + C_{it1}) + \frac{C_{it1}C_{Si}}{C_{BOX}} + \frac{qN_a t_{Si} C_{Si}}{C_{BOX(2\Phi_F)}}\right] + \frac{C_{NO}C_{Si}}{C_{BOX}(C_{Si} + C_{NO} + C_{it2})}(V_{FB\text{-}G2} - V_{g2\text{-}L}) + \frac{C_{it2}}{C_{BOX}} 2\Phi_F \frac{(C_{BOX} + C_{it1} + C_{Si})}{(C_{Si} + C_{NO} + C_{it2})} \quad (1)$$

In the above, C_{Si} is the capacitance of silicon thin film; $V_{FB\text{-}G1}$ is the substrate gate flat band voltage and $V_{FB\text{-}G2}$ is the secondary gate flat band voltage. In the present sensor structure contribution due to the $V_{FB\text{-}G2}$ term can be ignored because the secondary gate (that is over NO) is replaced by a molecular monolayer. C_{it1} and C_{it2} refer to interface state capacitance across the oxide at the BOX−Si interface and NO−Si interface, respectively. As there is no explicit secondary gate, $V_{g2\text{-}L}$ (L

for liquid phase) in the expression represents the electrolyte−oxide interface potential term in the case when the device is used as sensor in the liquid phase (also called zeta potential ψ_0).[23] The above equation is analyzed below for two different cases of interest: gaseous phase and liquid phase sensing applications. FDEC charge-coupled sensing is the means of signal transduction in gas phase sensing experiments discussed below. Whereas in the liquid phase pH sensing experiments both FDEC charge coupling and the regular Coulombic field-effect modulation of (minority) charge carriers take place, furthermore they compete with one other as they act in opposite directions; 50 μm × 600 μm Hall bar devices (Figure 4) were used to measure device response in liquid phase pH sensing experiments, and 10 μm × 20 μm devices (Figure 5) and submicrometer wires etched on Hall bar (50 μm × 600 μm) devices (Figure 3) were used to measure response in gas phase sensing experiments.

EXPERIMENTAL RESULTS

Gas Phase Sensing of Amine Molecules: Selective coordination of electron-donating ligand molecules at the metal atom centers of metalloporphyrin molecular monolayer has been used to demonstrate gas phase analyte molecule detection. For this purpose, ZnTCPP molecular monolayer was deposited on the native oxide surface using the Langmuir−Blodgett (LB) film deposition technique. Pyridine and piperidine molecules axially bind at the positively charged Zn^{2+} center of the planar zinc porphyrin molecules, resulting in the formation of a coordination complex, whereby the amine molecule donates an extra pair of electrons to the Zn^{2+} atom. Characterization of gas phase binding of amine molecules to the ZnTCPP monolayer was done using UV absorption spectroscopy. The results from these and other control experiments that demonstrate chemistry and selectivity of ligand binding on glass substrates, single monolayer coating of the device surface using LB technique, selective electrical response of large area devices (10 μm × 20 μm, 100 nm thickness), sensitivity (resolution) of detection up to few 100 attomoles of bound amine molecules, along with light resetting ability of devices have been discussed and analyzed in detail elsewhere.[14] Here, we present results from gas phase amine sensing experiments using quantum wire devices coated with ZnTCPP monolayer. Quantum wire (QW) devices with widths ranging from 100 to 500 nm were fabricated on large 50 μm × 600 μm Hall bar devices (100 nm thick) by EBL patterning followed by CF4 RIE etching. Gas phase amine sensing experiments using QWs of narrow widths (below 250 nm) did not yield reproducible results, with some devices showing no response to amine molecules, whereas experiments using 500 nm wide (and above) QW devices gave reproducible and consistent results. One possible reason for this might be due to failure in forming of a good quality ZnTCPP monolayer film using LB technique due to the high aspect ratio of the narrow width devices. Results from amine sensing experiments with 500 nm × 5 μm QW devices using pyridine and piperidine molecules are plotted in Figure 3.

Donation of the lone pair of electrons by pyridine and piperidine molecules to the heavily conjugated ZnTCPP porphyrin macrocycle results in an increase in the effective electron charge on the porphyrin monolayer. This sheet of extra negative charge on the device native oxide surface due to amine molecule binding causes capacitive discharging of electrons from interface trap states at the NO−Si interface, which in turn leads to a decrease in threshold voltage and an exponential increase in inversion drain current at the back interface of the n-channel MOSFET device. The high sensitivities of amine molecule detection that have been observed, up to few tens of parts per billion (PPB) of pyridine detection (Figure 3a) and up to a few parts per trillion (PPT) of piperidine detection (Figure 3b,c), are explained by the fully depleted exponential charge-coupling mechanism. Also, the equilibrium constants for pyridine and piperidine binding at ZnTCPP are 6300 and 112 000, respectively. These values are much lower than those for most other commonly used analyte species for sensor characterization experiments, where binding is essentially irreversible. The sensitivities observed in our experiments using pyridine and piperidine vapors assume larger significance,[24] in this context.

FDEC Charge-Coupled Sensor. Considering eq 1 for $V_{t\text{-}sub}$ to obtain a quantitative understanding of the proposed charge-coupling mechanism, we can deduce that only the last term in the right-hand side expression is of major significance. V_{FB1} is invariant, and the variation in $V_{t\text{-}sub}$ due to the second term in the expression is negligible as $C_{NO} \gg C_{it2}$. Addition of charge at the native oxide surface also lowers its surface work function (secondary gate work function Φ_{M2}), and consequently, V_{FB2} decreases (by 0.2 eV).[25] However, due to the fact that the charge added to the molecular monolayer is expected to be essentially immobile (it only changes the dipole moment of the molecules), the contribution of the V_{FB2} term can be ignored in this analysis. The $V_{g2\text{-}L}$ term is relevant only when the device is exposed to liquid solutions and will be considered later in the discussion. Analyzing the last term in the expression, for the case of gaseous phase sensing, we have

$$\Delta V_{t\text{-}sub} \sim qE_1 \frac{\Delta N_{it2}}{C_{NO}} \tag{2}$$

where ΔN_{it2} is the change in interface state density, and E_1 is the device charge-coupling amplification factor defined as

$$E_1 = \frac{2\Phi_F}{C_{BOX}} \frac{(C_{BOX} + C_{it1} + C_{Si})C_{NO}}{(C_{Si} + C_{NO} + C_{it2})} \sim \frac{2\Phi_F(C_{it1} + C_{Si})}{C_{BOX}} \tag{3}$$

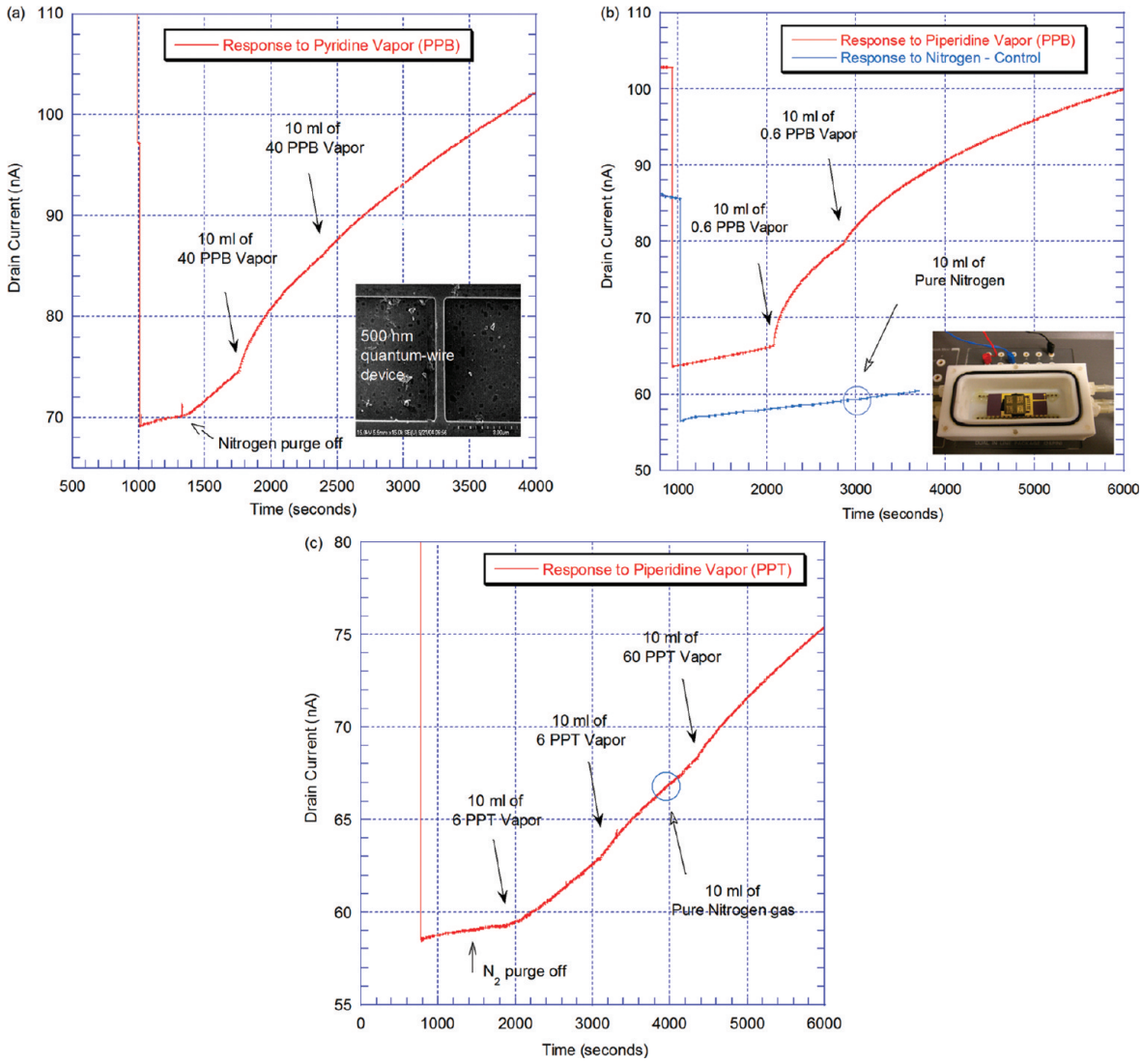

Figure 3. (a) Response of a 500 nm wide device coated with ZnTCPP. Saturated pyridine vapor was diluted 10^5 times with nitrogen, and 10 mL amount of this was introduced into Teflon cell enclosing the device. Device response to two aliquots introduced 10 min apart is shown. The vertical drop in drain current due to device resetting using LED light incidence and nitrogen purge is explained in ref 14. Inset shows FESEM image of a 500 nm device. (b) Response of 500 nm wide device to piperidine vapor diluted 10^7 times with nitrogen (red curve). Device does not exhibit any significant response to pure nitrogen (control), plotted in blue. The large response of device relative to the plot in (a) is understood to be due to higher binding constant and larger base strength of piperidine compared to pyridine. Inset shows picture of 50 mL internal volume Teflon cell assembly (cap off) with wire bonded device, integrated inside a HP test fixture. (c) Response of 500 nm wide device to piperidine vapor diluted 10^9 times with nitrogen (red curve). Two 10 mL aliquots of 6 PPT vapor, followed by pure nitrogen and 60 PPT vapor (10^8 times diluted) are introduced. A detailed study of amine sensing is discussed elsewhere.[14]

To get a rough estimate of the numbers, in our case of boron-doped (10^{15} cm^{-3}, $\Phi_F \sim 0.3$ eV) thin film silicon (100 nm) SOI MOSFET with 400 nm thick BOX and approximate interface state density (assumed) of 5×10^{11} cm^{-2} at the Si−BOX interface, amplification factor is calculated to be $E_1 \sim 13$. If $\Delta N_{it2} = 1 \times 10^{12}$ cm^{-2} and $C_{NO} \sim 17.2 \times 10^{-7}$ F cm^{-2}, $(q\Delta N_{it2}/C_{NO}) \sim 0.093$. Hence, the shift in threshold voltage of the inversion channel formed at the Si−BOX interface is $\Delta V_{t\text{-}sub} \sim 1.2$ V. When the surface of a fully depleted device biased in weak inversion (subthreshold region) is exposed to ligand molecules, as in the amine sensing experiments, added negative charge at the native oxide surface causes amplified modulation of device threshold voltage and drives it into strong inversion regime, resulting in an exponential gain in drain current response by a factor of 10 or more. This unique exponential coupling of the device response to the surface charge imparted by the target species in a monolayer floating gate, fully depleted SOI MOSFET leads to terming of the device structure as a fully depleted exponentially coupled (FDEC) sensor.

Liquid Phase pH Sensing. The delineation between regular MOSFET (inversion)-type field-effect response, termed "Coulombic" response hereafter, and the proposed FDEC response become apparent when the device with bare native oxide is exposed to aqueous buffer solutions of varying pH. The active surface (50

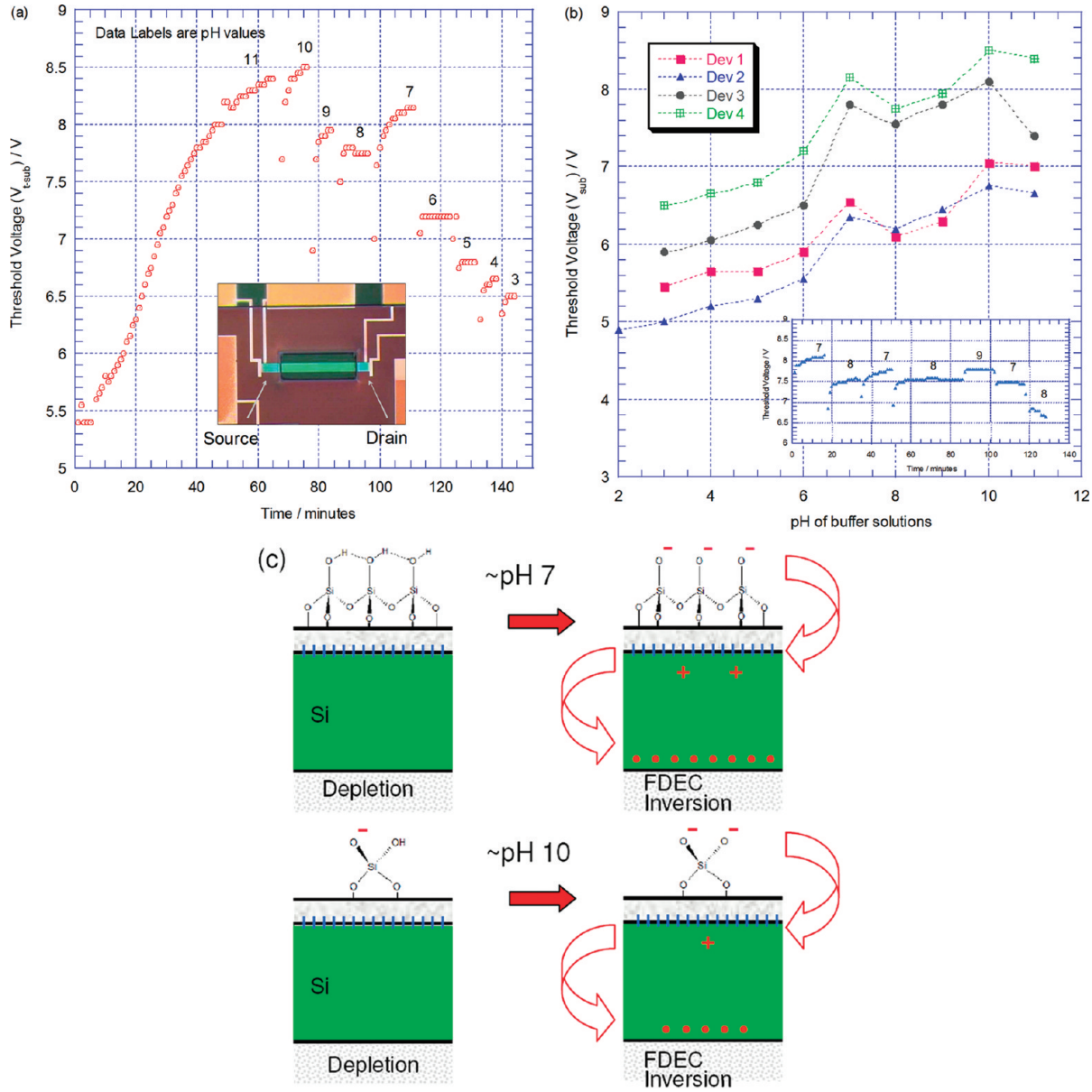

Figure 4. (a) Well encapsulated 50 μm × 600 μm Hall bar device with a 150 μm × 450 μm SU8 window (inset) is exposed to pH buffer solutions. Measured threshold voltage variation of the device with pH value of solution is plotted *vs* time. Data labels in the plot are pH values. The device exhibits anomalous shifts transitioning from pH 8 to pH 7 and from pH 11 to pH 10, where the threshold voltage increases, in opposite direction compared to other pH transitions. (b) Threshold voltage variation plotted against pH value of buffer solution for four different devices. All devices exhibit anomalous responses when transitioning from pH 8 to pH 7 and from pH 11 to pH 10. In the inset is plotted device threshold voltage response *vs* time when the device is exposed alternately to pH 7 and pH 8 (also pH 9) buffer solutions. The anomalous response is seen both ways, from acidic to basic solutions and *vice versa*. (c) Schematic of single (vicinal) silanol and double silanol (geminal) groups on native oxide surface, and formation of negative charge on oxide surface at anomalous pH points.

μm wide × 600 μm long) of a well-packaged device was treated with buffered oxide etch, dried in nitrogen, and fresh native oxide was grown in clean-room ambient conditions.[26] Threshold voltage of the device was defined arbitrarily in these experiments as the substrate bias corresponding to an inversion drain current of 10 nA. Device native oxide surface was exposed to different pH buffer solutions, and threshold voltage was measured with time by maintaining the drain current constant at 10 nA while varying the substrate bias (gate voltage) using a feedback circuit. Threshold voltage variation with time as the device is exposed to different pH buffer solutions is plotted in Figure 4a.

In typical FET-based sensor structures, a gradual (linear or nonlinear) unidirectional variation in threshold voltage is observed going from pH 11 to pH 3,[5,7,10] which in the case of n-channel MOSFET sensors is a gradual decrease in the threshold voltage, or equivalently decrease in sheet resistance. Whereas, in our experiments when using the FDEC sensor, the device exhibits anomalous shifts at two pH transition points. In Figure 4a at pH 8−7 and pH 11−10, the direction of

threshold voltage shifts at these transition points is opposite to the rest of the data and various reports in literature. The anomalous shifts at these two transition points occurred both ways (inset in Figure 4b), when going from buffer solutions with lower pH values (acidic) to higher pH values (basic) and *vice versa*. This anomalous behavior has been observed consistently in all experiments using at least six different devices. Threshold voltage variations with pH of buffer solutions from experiments using four different devices are plotted in Figure 4b. We initially attributed these anomalies as errors due to imperfections in the experimental setup. Even though the observed nonlinearity in response can be explained by considering chemical oxidation and reduction of the hydroxyl-terminated native oxide surface,[27,28] the anomalies at pH 7−8 and pH 10−11 cannot be explained by any of these well-understood and established concepts. In the discussion below, device threshold voltage variation with respect to increase in pH values of buffer solutions, that is, going from acidic to basic solutions, is analyzed for sake of convenience.

The observed anomalous threshold voltage response can be understood as the cumulative of two different, oppositely acting effects on the inversion channel carriers: the Coulombic effect due to electrolyte−native oxide interface potential ($V_{g2\text{-}L} = \psi_0$ in eq 1) and the proposed FDEC effect due to charge addition to the native oxide surface. The Coulombic effect in a regular MOSFET-type sensor is a function of ψ_0[29] and produces an increase in threshold voltage of electron inversion channel with decrease in $[H^+]$ ion concentration of the solution, from pH 2 to pH 12. It is explained using the site binding[30] and the site dissociation models.[31]

To explain the FDEC charge-coupling effect, we need to consider the surface terminal groups on the device native oxide surface and the corresponding surface charge due to their reactivity in pH buffer solutions. The native oxide formed on the active silicon surface is known to have various different terminating molecular groups, *viz.* single silanol (≡SiOH) groups (isolated and vicinal ends), double silanol groups ═$Si(OH)_2$ (germinal ends) and ≡Si−O−Si≡ bridge bonds.[32] When exposed to basic buffer solutions, the SiOH ends are deprotonated to form SiO^- ion-terminated ends, depending on the pH value of the buffer solution. The cumulative density of these surface hydroxyl groups is expected to depend on the surface preparation method and has been reported to vary from 0.8 to 8 groups per nm^{-2},[33] with a majority of them being single silanol groups. The dissociation constant for deprotonation of single silanol groups is $pK_a \sim 7$ (reports range from 6.5 to 7.5) and for deprotonation of the second OH group on double silanol (═SiO^-OH) is $pK_a \sim 9.8$ (reports range from 9.3 to 10), approximately.[34−36] Hence, at the two anomalous transition points (pH 7−8 and pH 10−11), changing of buffer solution to higher basic strength results in large increases in negative charge terminations at the native oxide surface (Figure 4c),[37] along with a corresponding decrease in $V_{g2\text{-}L}$.[38] This net increase in negative charge terminations at the native oxide surface (immobile charge, as defined by electrical double layer and triple layer models for electrolyte−solid interfaces) mirrors an increase in positive charge at the NO−Si film interface due to the high capacitance of native oxide, resulting in loss of electrons from the interface trap states and hence decrease in device threshold voltage. At the same time, the corresponding decrease in electrolyte−NO interface potential ($V_{g2\text{-}L}$) causes an increase in threshold voltage due to Coulombic depletion of charge carriers (electrons) far inside the silicon channel. The net result is *cumulative of the two competing effects*: the decrease in $V_{g2\text{-}L}$ that tends to cause an increase in threshold voltage (Coulombic effect) *versus* the FDEC effect due to increased negative charge on the oxide surface that tends to produce a decrease in threshold voltage.

$$\equiv SiOH \xleftrightarrow{\text{pH 7} \leftrightarrow \text{pH 8}} \equiv SiO^- + H^+$$

$$=SiO^-(OH) \xleftrightarrow{\text{pH 10} \leftrightarrow \text{pH 11}} = SiO_2^{2-} + H^+$$

In contrast, when the native oxide surface was functionalized with aminopropyltriethoxysilane (APTES) molecules, the anomalies in threshold voltage response were not observed,[27] similar to linear *versus* nonlinear pH response of nanowire devices reported by Cui *et al.*[5] APTES molecule binding consumes most of the surface silanol groups, resulting in no observed FDEC capacitive charge coupling. However, the amine end ($pK_a \sim 9.5$) of the APTES molecules is free to undergo proton exchange, but the net charge formed at the amine ends does not show any explicit FDEC-type threshold voltage decrease. This may be due to the screening of this charge by the solvent molecules along with the reduced capacitance in this case between charges at the amine ends and interface states at the NO−Si interface.

Liquid Phase Analytical Model, FDEC Potential Coupling. While evaluating the sensing response of the device in the liquid phase, the $V_{g2\text{-}L}$ term in eq 1 for $V_{t\text{-}sub}$ needs to be taken into account. The $V_{g2\text{-}L}$ term denotes the electrolyte−insulator interface potential ψ_0 (zeta potential) in this configuration.[29] In a fully depleted field-effect sensor structure, even the Coulombic field-effect modulation of channel carriers by the electrolyte−oxide interface potential $V_{g2\text{-}L}$ is amplified exponentially when compared to a partially depleted device structure. Elibol *et al.* have reported a similar analysis using a double gated thin film SOI FET structure.[39] In our case of n-channel FDEC sensor structure, threshold voltage variation with electrolyte−oxide interface potential can be written as

$$\Delta V_{t\text{-}sub} \sim E_2 \Delta V_{g2\text{-}L} \quad (4)$$

where the amplification factor for electrolyte−oxide interface potential E_2 is given by

$$E_2 = -\frac{C_{NO}C_{Si}}{C_{BOX}(C_{Si} + C_{NO} + C_{it2})} \sim -\frac{C_{Si}}{C_{BOX}} \quad (5)$$

The amplification factor is negative in the above equation because a decrease in $V_{g2\text{-}L}$ (ψ_0) produces an increase in $V_{t\text{-}sub}$. Also to be noted is that E_2 is relatively independent of interface trap state densities. Using the device parameters, E_2 for our device can be calculated to be ~12. For pH buffer solutions, the electrolyte−oxide interface potential (zeta potential) changes by a theoretical maximum of 0.059 V per unit change in pH at 298 K.[23] This translates to a maximum device threshold voltage variation of $\Delta V_{t\text{-}sub} \sim 0.7$ V per unit pH change due to amplification, for our FDEC device. This amplified response may explain the large amplitude changes in threshold voltage transitioning from pH 6 to pH 7 in our experiments, compared to reports of similar experiments with other structures.

Additionally, referring to eq 1 for $V_{t\text{-}sub}$, since $\Delta V_{FB2} \sim \Delta\Phi_{M2}$, where Φ_{M2} is the work function of a chemical sensitive thin film deposited on the active surface of the device, the device can also be used to sense work function changes caused by target molecule interactions.[40] This is the case when a decrease in Φ_{M2} is accompanied by formation of free charge carriers (electrons that are mobile) in the chemical sensitive film, where electron transfers occur from the chemical-sensitive film to the fully depleted silicon, resulting in energy bands bending downward in the silicon film causing a flush of extra electrons in the channel (similar to functioning of a MESFET) and hence resulting in a decrease in the threshold voltage of inversion channel ("MESFET"-type response, hereafter). In our gas phase amine binding experiments, work function of the porphyrin monolayer decreases but is accompanied only by a change in dipole moment of the porphyrin molecules (porphyrin−amine coordination complex). There is no free charge on the porphyrin monolayer due to amine binding, hence we do not expect any substantial contribution due to the MESFET-type effect. Therefore, FDEC charge-coupling effect due to capacitive interface state coupling (as explained previously) is expected to be the main cause of the observed gas phase amine binding response.

From eq 1, it can be deduced that the fully depleted device amplification factor for MESFET-type response is $-E_2 \sim (C_{si}/C_{BOX})$, as a decrease in Φ_{M2} results in a decrease in $V_{t\text{-}sub}$. However, the presence of interface trap states at the NO−Si interface reduces the sensitivity of device to free charge addition on the chemical-sensitive film. Hence, interface trap states and other defects need to be reduced when the device is used as a sensor in this MESFET-type configuration to avoid secondary effects.

Cumulative change in substrate threshold voltage ($\Delta V_{t\text{-}sub}$) due to all the different contributions can hence be written as

$$\Delta V_{t\text{-}sub} \sim qE_1 \frac{\Delta N_{it2}}{C_{NO}} + E_2(\Delta V_{g2\text{-}L} - \Delta\Phi_{M2}) \quad (6)$$

Numerical Simulations. To further understand and validate the concepts and the theoretical framework presented above, we modeled the working of the device using Atlas numerical simulations software (Silvaco Corp). Owing to the complex nature of interactions at the various interfaces of the sensor device and within the inverted silicon channel, caused by target molecule binding at the chemical-sensitive film in such hybrid semiconductor device structures with organic−inorganic interfaces, and the relative high level of difficulty in exact modeling of these, we have developed a simplified model that represents these complex interactions using the modeling tools available in Atlas device simulation software. We present here a simple model, an alternative model to the one we previously presented,[14] that simulates the capacitive charge coupling, potential coupling, and the work function coupling interactions within the MOSFET sensor device and validates the FDEC theory to explain the results obtained in our experiments. This simplistic model extended here is to be viewed in terms of a proof of concept, validating and enabling understanding of the sensing mechanisms delineated above. A more exact simulation model involving molecular orbital coupling with interface states and the energy band levels in silicon needs to be developed to better understand the device physics[41] and forms part of the future work.

A SOI MOSFET device (Figure 5) of 10 μm length, 100 nm channel thickness, and 1 μm width controlled by substrate silicon acting as gate was defined using the simulation parameters listed in Table 1. The native oxide layer is modeled as a 2 nm thick thermal oxide on the silicon channel region, and the ZnTCPP porphyrin monolayer is modeled by defining a 2 nm thin semiconducting layer (with parameters similar to intrinsic silicon) on top of the native oxide, while isolated from the source−drain regions at either ends (by 100 nm) to avoid conductance through the 2 nm film. The use of a semiconducting thin film to model ZnTCPP monolayer is due to the reported semiconducting nature of porphyrin molecules in both thin film and bulk solid phases.[42,43] Interface trap states are defined separately at each of the two interfaces, above and below the silicon channel, using Gaussian profiles as plotted in Figure 5a. Lower fixed oxide charge density value at the NO−SOI interface is used in order to optimize the simulated FDEC response. Also donor states at the NO−SOI interface above the Fermi level act equivalent to fixed

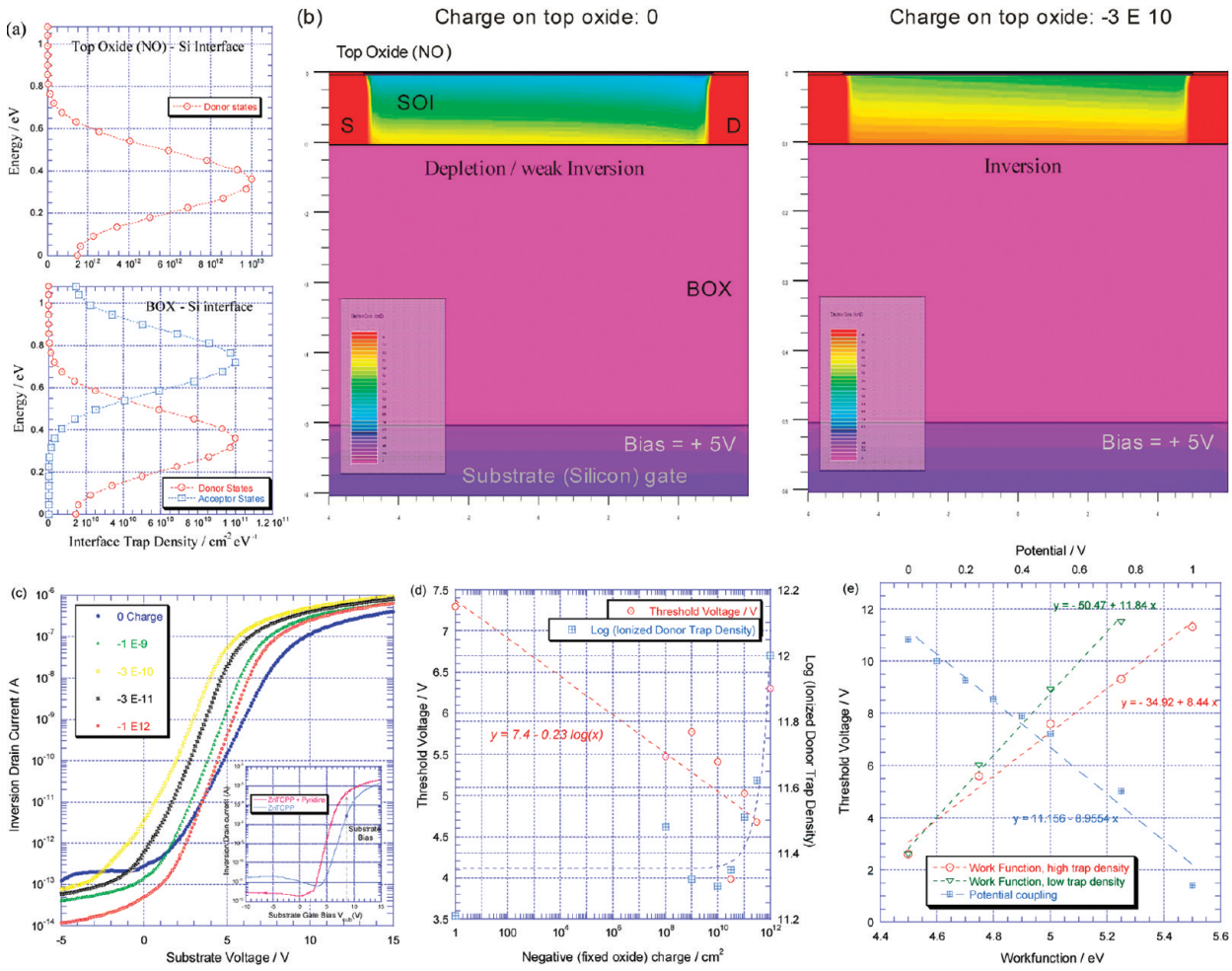

Figure 5. (a) On the top is plotted interface state density profile defined at the top oxide (NO)−Si interface. Donor-type trap states are used as they are expected to interact (FDEC) most below the Fermi level in our boron-doped SOI. Below is plotted donor and acceptor state profiles defined at the Si−BOX interface. (b) Two-dimensional electron density distribution (Tonyplot, Atlas) plot with no charge (left) defined at the 2 nm model porphyrin semiconducting film−top oxide (NO) interface, and with -3×10^{10} cm^{-2} fixed oxide charge defined at the interface (right). Addition of negative fixed oxide charge simulates the amine molecule binding at ZnTCPP monolayer in our experiments. Red color in the plot corresponds to electron density of 10^{18} cm^{-3}, and pink color to 10^{3} cm^{-3}. As can be seen, addition of charge on the top oxide induces inversion at the Si back channel $\sim 10^{12}$ cm^{-2}, an order of magnitude higher charge density relative to negative fixed oxide charge added on top. (c) Numerically simulated I_d-V_g curves for varying negative fixed oxide charge densities added at the model porphyrin film−top oxide (NO) interface. Data labels are density per cm^2. Experimental drain current curves before (blue) and after (red) pyridine binding at ZnTCPP monolayer (ref 14) are plotted in the inset. Drain current crossover going from depletion to inversion, and corresponding decrease in threshold voltage can be seen. These characteristics are reproduced in the numerical simulations. (d) Numerically simulated threshold voltage variation plotted against negative fixed oxide charge density. Log of ionized donor trap density at the top oxide−Si interface is plotted on the secondary *y*-axis. (e) Numerically simulated threshold voltage variation with change in floating gate (defined at the model porphyrin film−top oxide interface) work function and potential (secondary *x*-axis). Work function variation with high (10^{13} cm^{-2} eV^{-1}) and low (10^{12} cm^{-2} eV^{-1}) interface state density, at the top oxide−NO interface is plotted. Slope of linear fit(s) agrees well with the rough estimate of E_2 obtained in the previous section.

oxide charges. A drain current *versus* (substrate) gate bias characteristic curve (blue curve in Figure 5c) before binding of the target molecules onto the chemical sensitive film, similar to that measured in our experiment (inset Figure 5c, blue curve), is obtained by varying the fitting parameters listed in Table 1.

As discussed in the previous sections, amine molecule binding at the ZnTCPP porphyrin monolayer causes an effective increase in the negative charge on the porphyrin monolayer, producing a resultant increase in (electron) inversion channel current. In our simulations, this effective increase in negative charge due to target molecule binding events is modeled by the addition of *excess "negative fixed oxide charge" at the model monolayer−native oxide interface*, whereby this negative fixed oxide charge added on top of the native oxide is capacitively coupled with the interface trap states at the native oxide−silicon channel interface, simulating the proposed FDEC charge-coupling mechanism. Negative fixed oxide charge is used to simulate the negative charge on molecular monolayer due to the immobile nature of the fixed oxide charge, compared to simulating it by changing the work function of the model porphyrin semiconducting thin film (or a float-

TABLE 1. Numerical Simulation Parameters Used for Modeling the Fully Depleted SOI FET Device Using Atlas Software (Silvaco Corp)

atlas simulation parameter	value
SOI channel thickness	100 nm
SOI device, length × width	10 μm × 1 μm
buried oxide thickness	400 nm
SOI channel doping	p-type (boron), 10^{15} cm^{-3}
model porphyrin semiconducting film (2 nm)	
electron affinity	4.9 eV
DOS[a] at 300 K (in valence and conduction bands)	10^{14}
fixed oxide charge density	
at SOI channel-native oxide interface	1×10^{8} cm^{-2}
at SOI channel-buried oxide interface	1×10^{9} cm^{-2}
at buried oxide-silicon substrate interface	1×10^{11} cm^{-2}
interface trap density, N_{it}	
at SOI channel−native oxide interface	1×10^{13} cm^{-2}
($E_V - E_{GD}$[b] = 0.35, 25 degenerate levels)	(donors, Gaussian profile)
at SOI channel−buried oxide interface	2×10^{11} cm^{-2}
($E_V - E_{GD}$[b] = 0.35, $E_C - E_{GA}$ = 0.35, 25 levels)	(equal donors and acceptors, Gaussian profile)

[a]DOS, density of states. [b]E_v, valence band energy; E_{GD}, peak energy of Gaussian profile.

ing gate) where transfer of charge carriers invariably occurs. For this reason, to improve the effectiveness of simulating charge coupling using negative fixed oxide charge to model target molecule binding, electronic band parameters of the 2 nm thick model porphyrin semiconducting thin film are defined such that the interactions between the carriers and energy states inside the 2 nm thin film, with the interface states and the charge carriers in the silicon channel are minimized (electron affinity of 4.9, and density of states (DOS) at 300 K of 10^{14}, in both valence and conduction bands).

By incrementally increasing the negative fixed oxide charge density defined at the model monolayer−native oxide interface, representing gradual amine molecular binding with time at the ZnTCPP chemical sensitive monolayer, back channel drain current *versus* (substrate) gate bias curves for drain−source bias of 0.1 V are numerically simulated, while keeping all other parameters constant. It is to be noted that amine molecule binding at the ZnTCPP molecule is expected to form an electrical dipole on the amine−ZnTCPP coordination complex, with partial charge polarization of either moieties. The charge simulated here by defining the negative fixed oxide charge is the cumulative of these partial charge densities on the molecular monolayer. Hence, any defined negative fixed oxide charge density might correspond to as much as a 10-fold target (amine) molecule binding density at the chemical-sensitive device surface. Numerically simulated drain current curves for negative fixed oxide charge density values ranging from 10^{9} to 10^{12} cm^{-2} are plotted in Figure 5c.

Threshold voltage shifts of the simulated curves from the initial (threshold voltage corresponding to no binding of target amine molecules) are plotted in Figure 5d against the negative fixed oxide charge defined at the model monolayer−native oxide interface. In the same figure on the secondary *y*-axis is plotted the cumulative positive charge due to charging and discharging of interface states at the native oxide−silicon channel interface (at initialization, zero bias condition), caused by the capacitive coupling of these interface states with the negative fixed oxide charge added at the simulated monolayer−native oxide interface. As can be seen from plot in Figure 5d, the decrease in simulated threshold voltage with increase in negative fixed oxide charge is not a monotonous function. This may be due to the complex nature of interactions between the added negative fixed oxide charges, interface trap states defined at the top oxide−silicon channel interface, valence and conduction band states in the model semiconducting porphyrin layer, the electron states in silicon channel, *etc.* and the resulting inaccuracies associated with the initialization and convergence of numerical simulations. It can be seen that addition of -3×10^{10} cm^{-2} fixed oxide charge produces over 3 orders of magnitude increase in drain current when biased in weak inversion regime. This corresponds to a density of fewer than two charges per 100 nm^2 area, or an order of magnitude increase in drain current corresponds to less than two charges per 1 μm^2 area. Hence, a 10 μm length × 100 nm width nanowire FDEC device is expected to detect unit charge additions, target binding events on the device surface, with up to an order of magnitude increases in device drain current.

A linear fit of simulated data (excluding last data point) yields a threshold voltage lowering of 0.23 V per 1 order increase in negative fixed oxide charge density for the set of parameters listed in Table 1, provided the minimum fixed charge density defined is within a few orders of that corresponding to the ionized interface and surface states (to avoid charge screening). As the negative fixed charge density is increased further, above 10^{11} cm^{-2}, the simulated threshold voltage of the device begins to increase. This is expected to occur when Coulombic effect due to added negative fixed oxide charge offsets the FDEC effect due to interface state charge coupling, when the effective capacitance across the top oxide (NO) due to interface trap states falls low compared to the increased negative fixed oxide charge density, whereby the latter directly modulates the inversion charge density at the BOX−Si interface.

Comparing the measured device $I_d - V_g$ curves before and after exposure to amine molecules, the experimental data plotted in the inset of Figure 5c, we observe that the curves exhibit a *crossover* at 3 V substrate gate bias. This crossover point is expected to occur when conductance in the Si channel transitions from depletion regime to inversion regime, with inversion channel formed at the BOX−Si channel interface, fur-

ther confirming the FDEC theory. When the silicon channel is operated in partially depleted or fully depleted mode (no inversion), Coulombic field effect due to added negative fixed oxide charge decreases the minority charge carrier (electrons) conductance in the silicon channel, whereas when it is biased in inversion, the threshold voltage decreases or the silicon channel conductance (of inversion electrons) increases due to the proposed FDEC interface charge-coupling effect. Hence, the two curves crossover, and the red curve is shifted left at the onset of inversion, resulting in lower threshold voltage after binding of the target (amine) molecules. The same behavior is reproduced in the simulated I_d-V_g curves plotted in Figure 5c, the crossover of the blue colored curve (initial) with all the other curves, and the crossover characteristic becomes more and more significant with higher negative fixed oxide charge densities, as expected. The exponential increase in drain current, the associated threshold voltage shift, and the crossover at the onset of inversion form the defining characteristics of FDEC charge-coupling sensor device.

In order to simulate the potential coupling and the work function coupling described in the previous section, a floating gate electrode that is isolated from source drain regions (by 100 nm on either side) was defined at the model 2 nm porphyrin semiconducting thin film−top oxide interface. The negative fixed charge at the interface was defined to be zero, with all other parameters being the same. The variation of the device threshold voltage with floating gate potential calculated from the numerically simulated I_d-V_g curves is plotted in Figure 5e (top *x*-axis). A linear fit to the simulated threshold voltage shifts yields a slope of −8.95, with the negative sign representing a lowering of threshold voltage with increase in potential applied over the top oxide. This agrees well with the rough estimate of the E_2 value (12) for potential coupling obtained in the previous section. In a similar manner, variation of device threshold voltage with work function of the floating gate electrode is plotted in the same figure (bottom *x*-axis), with high and low interface trap state density at the top oxide (NO)−Si interface, while keeping all other parameters constant. A linear fit of simulated threshold voltage shifts yields values of +8.44, and +11.84, which again agree reasonably well with the rough estimate of E_2 (12) attained previously for work function coupling. This amplified variation of threshold voltage of simulated I_d-V_g curves with potential and work function defined over the top oxide further confirms the analytical model presented in the previous section.

CONCLUSION

Selective binding of amine molecules at the positively charged Zn^{2+} centers on the ZnTCPP monolayer deposited on device native oxide surface has been demonstrated by comparing the responses of control devices coated with free-base TCPP, palmetic acid molecular monolayers, and devices with bare native oxide surface, presented previously.[14] Formation of a coordination complex between the amine molecules and the ZnTCPP molecules causes an order of magnitude larger increase in device drain current compared to that due to interactions between amine molecules and other control monolayers (nonspecific physiadsorption). We can hence deduce that a chemical reaction involving oxidation and reduction of molecular species and corresponding charge transfers (partial) on the device surface is essential for FDEC charge coupling to occur. This demonstrates the chemical-sensitive FDEC charge-coupled device as a *chemical reaction sensor*, wherein a chemical interaction at the device surface induces an inversion current in the drain channel.

One of the principle challenges with sensor devices is the rate of false positive and false negative generation and the economic and health costs associated with these errors, especially in automated, autonomous detection systems. An array of FDEC nanowire sensors with predesigned switching characteristics, acting as a single sensor unit, can be used to attain extreme selectivity along with ultrahigh sensitivity in detection of specific target species. A redundant combinatorial detection array (RCDA) containing four pairs of complementary n-channel and p-channel FDEC nanowire devices, all with same chemical-sensitive surface, operated with a pair each in enhancement mode, depletion mode, partial depletion with inversion mode and accumulation mode, will yield different preidentified responses from each device for a given target molecule detection. Such an example array of eight different nanowire devices exposed to test medium should give very low false positives. These arrays can be fabricated by simply varying the doping density of the SOI channel, varying threshold adjust implants or silicon film thickness, among other such fabrication parameters. ULSI planar manufacturing compatibility of these CMOS FDEC sensor devices enables SOC integration and low cost manufacturing of sensor chips containing millions of devices.

A higher order array of nested RCDAs, each RCDA coated with a unique dielectric material, molecular monolayer or chemical-sensitive thin film, combined with advanced pattern recognition using statistical techniques, cluster analysis or neural networks can be realized into highly capable electronic nose and tongue devices. An enhancement mode device exhibiting anomalous FDEC response at pH 7, when biased at the lower threshold voltage value, switches on at pH 8 and pH 6 but not at pH 7. FDEC device arrays coated with selected top dielectric materials,[35] chemical-sensitive films, with varying surface chemical terminations and respective oxidation−reduction potentials can be used for sensing unique pH values of solutions. Due to the

fact that FDEC charge coupling occurs at specific pH value of solution for a given surface chemistry of the device, these sensor arrays can be used as *reference-less pH sensors*.

METHODS

Device Fabrication: Starting material for the back gated SOI MOSFET transistors used in this work is a p-type SOI wafer (ρ = 2−10 $\Omega \cdot$ cm) with initial SOI film thickness of 200 nm and underlying buried oxide (BOX) layer thickness of 400 nm, sourced from IBIS Technology Corporation. The SOI channel thickness is thinned to 100 nm by wet oxidation at 1000 °C. Plasma-enhanced chemical vapor deposition (PECVD) is performed to further increase the oxide thickness and to obtain an effective oxide mask for phosphorus n+ doping. Buffered oxide etch (BOE) is used to open windows in the thick oxide layer for source−drain n+ doping. Phosphorus doping is carried out using phosphorus pentoxide solid source wafers in a diffusion furnace. The masking oxide is then removed by dipping the wafer in BOE for 15 min. Device isolation is attained by physical separation *via* reactive ion etching (RIE) of patterned silicon mesas using SF_6 etch chemistry. The wafer is then patterned to open windows in the buried oxide for deposition of a metal layer to enable electrical contact to the silicon substrate gate. BOE is used to etch away the buried oxide from the patterned openings. Metal contacts to substrate and devices are formed by deposition of 200 nm of aluminum, using a TorrVac electron beam evaporator. Bonding pads are formed by depositing 10 nm of chromium followed by 100 nm gold in an Edwards's thermal evaporator. Ten micrometer × 20 μm and large 50 μm × 600 μm Hall bar devices were fabricated using these conventional n-MOS process steps. Submicrometer quantum wire devices from 100 to 500 nm wide devices were formed on 50 μm × 600 μm bars by electron beam lithography (EBL) patterning of PMMA resist, followed by reactive ion etching (RIE) using CF_4 etch chemistry.

LB Porphyrin Monolayer Deposition: Zn(II) 5,10,15,20-tetra-(3-carboxylphenyl)porphyrin (ZnTCPP) monolayer deposition by the Langmuir−Blodgett technique has been done using a constant perimeter barrier type Joyce-Loebl Mini LB trough. Twenty micromolar solutions of porphyrin molecules are prepared by dissolving ZnTCPP in 2:1 mixture of dichloromethane and methanol. Porphyrin monolayers are formed in LB trough over a water subphase with a pH of 4.5, prepared using hydrochloric acid. The deposition of the porphyrin monolayer onto the device surface was done by very slow withdrawing of an immersed device, while applying a constant pressure of 20 mN $\cdot$ m^{-1} on the LB constant perimeter barrier.

Gas Phase Amine Sensing Experiments: Gas phase amine binding experiments were performed inside a custom-built Teflon cell, with inlets and outlets for pumping of analyte gases. Teflon cell was integrated with white LED for light exposure for device reactivation. Dilute amine vapors (pyridine and piperidine) were prepared by mixing pure nitrogen gas with saturated amine vapors formed over nitrogen gas in a conical flask. 0.5 mL of saturated amine vapor in a 5 mL disposable syringe was injected, mixed into 49.5 mL of pure nitrogen gas in a 50 mL syringe using disposable valve adaptors to yield 100 times diluted amine vapor. All syringes and valve adaptors were discarded after a single use. A repetition of the above method using new parts yielded 10 000 times diluted amine vapor, and so on. Each dilution step took about 5 min, much less than few hours' time scale for significant Brownian particle (molecular) absorption onto syringe tube walls. The device was illuminated with LED light (350 mW/cm^2 for 30 min),[14] followed by 10 mL aliquots of diluted amine vapors introduced into Teflon cell assembly and device response measured. A repetition of dilution and mixing process with no amine vapor but with just nitrogen gas when introduced showed no device response (blue curve in Figure 3b), while diluted pyridine and piperidine vapors showed consistent responses, that is, progressive lowering of device responses for higher dilutions and lower base strengths. Vapor pressures of pyridine (16 mmHg) and piperidine (25 mmHg) at NTP were used in sensitivity calculations.

Liquid Phase pH Sensing Experiments: For liquid phase experiments, device isolation and encapsulation were achieved by using a two-step process. First, 100 μm thick SU8 resist coating was used to open windows over active area of the device and over bonding pads to enable electric contact with external circuit; 50 μm × 600 μm large Hall bar devices were used for pH sensing experiments due to ease of isolation (inset Figure 4a). The device (die) was glued onto a chip carrier, and electric contacts were formed by gold wire bonding using ultrasonic ball-wedge bonder. As a second step of encapsulation, 5 min commercial epoxy glue was applied to cover bonding pad areas and all other electrical contacts to achieve electric insulation when testing with aqueous pH solutions. Fully encapsulated device with open windows over active device areas was treated with BOE solution, and fresh native oxide was grown in clean-room conditions. The device was inverted surface down, its surface thoroughly wetted with DI water and immersed into different pH buffer solutions, and drain current response was measured.

Acknowledgment. The author thanks Professor Trevor Thornton and Professor Devens Gust for helpful discussions, Drs. Gez M. Laws, Paul A. Liddell, Joakim Andre'asson, Yuichi Terazono, and Zach Erno for porphyrin monolayer deposition, characterization, and synthesis. This work was supported partially by the National Science Foundation, Award Nos. ECS0097434 and CHE-0352599.

REFERENCES AND NOTES

1. Schedin, F.; Geim, A. K.; Morozov, S. V.; Hill, E. W.; Blake, P.; Katsnelson, M. I.; Novoselov, K. S. Detection of Individual Gas Molecules Adsorbed on Graphene. *Nat. Mater.* **2007**, *6*, 652–655.
2. Armani, A. M.; Kulkarni, R. P.; Fraser, S. E.; Flagan, R. C.; Vahala, K. J. Label-Free, Single-Molecule Detection with Optical Microcavities. *Science* **2007**, *317*, 783–787.
3. Kemiktarak, U.; Ndukum, T.; Schwab, K. C.; Ekinci, K. L. Radio-Frequency Scanning Tunnelling Microscopy. *Nature* **2007**, *450*, 85–88.
4. Kong, J.; Franklin, N. R.; Zhou, C. W.; Chapline, M. G.; Peng, S.; Cho, K. J.; Dai, H. J. Nanotube Molecular Wires as Chemical Sensors. *Science* **2000**, *287*, 622–625.
5. Cui, Y.; Wei, Q. Q.; Park, H. K.; Lieber, C. M. Nanowire Nanosensors for Highly Sensitive and Selective Detection of Biological and Chemical Species. *Science* **2001**, *293*, 1289–1292.
6. Forzani, E. S.; Zhang, H. Q.; Nagahara, L. A.; Amlani, I.; Tsui, R.; Tao, N. J. A Conducting Polymer Nanojunction Sensor for Glucose Detection. *Nano Lett.* **2004**, *4*, 1785–1788.
7. Stern, E.; Klemic, J. F.; Routenberg, D. A.; Wyrembak, P. N.; Turner-Evans, D. B.; Hamilton, A. D.; LaVan, D. A.; Fahmy, T. M.; Reed, M. A. Label-Free Immunodetection with CMOS-Compatible Semiconducting Nanowires. *Nature* **2007**, *445*, 519–522.
8. Sysoev, V. V.; Button, B. K.; Wepsiec, K.; Dmitriev, S.; Kolmakov, A. Toward the Nanoscopic "Electronic Nose": Hydrogen *vs* Carbon Monoxide Discrimination with an Array of Individual Metal Oxide Nano- and Mesowire Sensors. *Nano Lett.* **2006**, *6*, 1584–1588.
9. Bergveld, P. Thirty years of ISFETOLOGY: What Happened in the Past 30 Years and What May Happen in the Next 30 Years. *Sens. Actuators, B* **2003**, *88*, 1–20.
10. Nikolaides, M. G.; Rauschenbach, S.; Bausch, A. R. Characterization of A Silicon-on-Insulator Based Thin Film Resistor in Electrolyte Solutions for Sensor Applications. *J. Appl. Phys.* **2004**, *95*, 3811–3815.

11. He, T.; Corley, D. A.; Lu, M.; Spigna, N. H. D.; He, J.; Nackashi, D. P.; Franzon, P. D.; Tour, J. M. Controllable Molecular Modulation of Conductivity in Silicon-Based Devices. *J. Am. Chem. Soc.* **2009**, *131*, 10023–10030.
12. Colinge, J.-P. *Silicon-On-Insulator Technology: Materials to VLSI*, 3rd ed.; Springer: Berlin, 2005.
13. Celler, G. K.; Cristoloveanu, S. Frontiers of Silicon-on-Insulator. *J. Appl. Phys.* **2003**, *93*, 4955–4978.
14. Takulapalli, B. R.; Laws, G. M.; Liddell, P. A.; Andreasson, J.; Erno, Z.; Gust, D.; Thornton, T. J. Electrical Detection of Amine Ligation to a Metalloporphyrin *via* a Hybrid SOI-MOSFET. *J. Am. Chem. Soc.* **2008**, *130*, 2226–2233.
15. Schroder, D. K.; Babcock, J. A. Negative Bias Temperature Instability: Road to Cross in Deep Submicron Silicon Semiconductor Manufacturing. *J. Appl. Phys.* **2003**, *94*, 1–18.
16. Ogawa, S.; Shimaya, M.; Shiono, N. Interface-Trap Generation at Ultrathin SiO_2 (4−6nm)−Si Interfaces During Negative-Bias Temperature Aging. *J. Appl. Phys.* **1995**, *77*, 1137–1148.
17. Stesmans, A. Low-Temperature Electron-Spin-Resonance Study of Pb0 Defects Residing in the (111) Si/Native Oxide Interface. *Appl. Surf. Sci.* **1987**, *30*, 134–141.
18. Stesmans, A. Structural Relaxation of Pb Defects at the (111)Si/SiO_2 Interface as a Function of Oxidation Temperature—The Pb-Generation-Stress Relationship. *Phys. Rev. B* **1993**, *48*, 2418–2435.
19. Poindexter, E. H.; Caplan, P. J.; Deal, B. E.; Razouk, R. R. Interface States and Electron-Spin Resonance Centers in Thermally Oxidized (111) and (100) Silicon-Wafers. *J. Appl. Phys.* **1981**, *52*, 879–884.
20. Balestra, F.; Brini, J.; Gentil, P. Deep Depleted SOI MOSFETs with Back Potential Control—A Numerical-Simulation. *Solid-State Electron.* **1985**, *28*, 1031–1037.
21. Hovel, H. J. Si Film Electrical Characterization in SOI Substrates by the HgFET Technique. *Solid-State Electron.* **2003**, *47*, 1311–1333.
22. Balestra, F.; Benachir, M.; Brini, J.; Ghibaudo, G. Analytical Models of Subthreshold Swing and Threshold Voltage for Thin-Film and Ultra-Thin-Film SOI MOSFETs. *IEEE Trans. Electron Dev.* **1990**, *37*, 2303–2311.
23. Olthuis, W. Chemical and Physical FET-Based Sensors or Variations on an Equation. *Sens. Actuators, B* **2005**, *105*, 96–103.
24. Dan, Y.; Lu, Y.; Kybert, N. J.; Luo, Z.; Johnson, A. T. C. Intrinsic Response of Graphene Vapor Sensors. *Nano Lett.* **2009**, *9*, 1472–1475.
25. Grover, R.; Carthy, B. M.; Zhao, Y.; Jabbour, G. E.; Sarid, D.; Laws, G. M.; Takulapalli, B. R.; Thornton, T. J.; Gust, D. Kelvin Probe Force Microscopy as a Tool for Characterizing Chemical Sensors. *Appl. Phys. Lett.* **2004**, *85*, 3926–3928.
26. Ashcroft, B.; Takulapalli, B.; Yang, J.; Laws, G. M.; Zhang, H. Q.; Tao, N. J.; Lindsay, S.; Gust, D.; Thornton, T. J. Calibration of a pH Sensitive Buried Channel Silicon-on-Insulator MOSFET for Sensor Applications. *Phys. Status Solidi B* **2004**, *241*, 2291–2296.
27. Takulapalli, B. R.; Thornton T. J. Gust; D. Ashcroft; B. Lindsay; S. M. Zhang; H. Q.; Tao, N. The pH Response of a Silicon-on-Insulator MOSFET with an Integrated Nanofluidic Cell. SOI Conference, IEEE International, 2003; pp 114−116.
28. Allen, L. H.; Matijevi, E; Meties, L. Exchange of Na^+ for Silanolic Protons of Silica. *J. Inorg. Nucl. Chem.* **1971**, *33*, 1293–1299.
29. VanHal, R. E. G.; Eijkel, J. C. T.; Bergveld, P. A General Model to Describe the Electrostatic Potential at Electrolyte Oxide Interfaces. *Adv. Colloid Interface Sci.* **1996**, *69*, 31–62.
30. Yates, D. E.; Levine, S.; Healy, T. W. Site-Binding Model of Electrical Double-Layer at Oxide−Water Interface. *J. Chem. Soc., Faraday Trans. 1* **1974**, *70*, 1807–1818.
31. Bousse, L.; Derooij, N. F.; Bergveld, P. Operation of Chemically Sensitive Field-Effect Sensors as a Function of the Insulator−Electrolyte Interface. *IEEE Trans. Electron Dev.* **1983**, *30*, 1263–1270.
32. Legrand, A. P. *The Surface Properties of Silicas*; John Wiley & Sons: New York, 1998.
33. Fisk, J. D.; Batten, R.; Jones, G.; O'Reilly, J. P.; Shaw, A. M. pH Dependence of the Crystal Violet Adsorption Isotherm at the Silica−Water Interface. *J. Phys. Chem. B* **2005**, *109*, 14475–14480.
34. Zhdanov, S. P.; Kosheleva, L. S.; Titova, T. I. IR Study of Hydroxylated Silica. *Langmuir* **1987**, *3*, 960–967.
35. Hair, M. L.; Hertl, W. Acidity of Surface Hydroxyl Groups. *J. Phys. Chem.* **1970**, *74*, 91–94.
36. Dijkstra, T. W.; Duchateau, R.; van Santen, R. A.; Meetsma, A.; Yap, G. P. A. Silsesquioxane Models for Geminal Silica Surface Silanol Sites. A Spectroscopic Investigation of Different Types of Silanols. *J. Am. Chem. Soc.* **2002**, *124*, 9856–9864.
37. Carroll, S. A.; Maxwell, R. S.; Bourcier, W.; Martin, S.; Hulsey, S. Evaluation of Silica−Water Surface Chemistry Using NMR Spectroscopy. *Geochim. Cosmochim. Acta* **2002**, *66*, 913–926.
38. Hayes, K. F.; Leckie, J. O. Modeling Ionic-Strength Effects on Cation Adsorption at Hydrous Oxide−Solution Interfaces. *J. Colloid Interface Sci.* **1987**, *115*, 564–572.
39. Elibol, O. H.; Reddy, B.; Bashir, R. Nanoscale Thickness Double-Gated Field Effect Silicon Sensors for Sensitive pH Detection in Fluid. *Appl. Phys. Lett.* **2008**, *92*, 193904.
40. Cahen, D.; Hodes, G. Molecules and Electronic Materials. *Adv. Mater.* **2002**, *14*, 789–798.
41. Braun, S.; Salaneck, W. R.; Fahlman, M. Energy-Level Alignment at Organic/Metal and Organic/Organic Interfaces. *Adv. Mater.* **2009**, *21*, 1450–1472.
42. Savenije, T. J.; Goossens, A. Hole Transport in Porphyrin Thin Films. *Phys. Rev. B* **2001**, *64*, 115323.
43. Harima, Y.; Takeda, K.; Yamashita, K. Molecular-Solid of Zinc Tetraphenylporphyrin as a Model Organic Semiconductor with a Well-Defined Depletion Layer. *J. Phys. Chem. Solids* **1995**, *56*, 1223–1229.